J. Fluid Mech. (1997), *vol.* 339, *pp.* 239–260

Copyright © 1997 Cambridge University Press

Global linear stability analysis of thin aerofoil wakes

By B. M. WOODLEY AND N. PEAKE

Department of Applied Mathematics and Theoretical Physics, University of Cambridge, Silver Street, Cambridge, CB3 9EW, UK

(Received 13 August 1996 and in revised form 17 January 1997)

We investigate the global linear stability properties of the quasi-parallel flow in the neighbourhood of the trailing edge of a thin aerofoil, using a WKBJ/multiple scales formulation in the limit of large Reynolds number, as originally developed by Monkewitz, Huerre & Chomaz. We show that the wake is globally linearly unstable to second order in the asymptotic expansion parameter at all Reynolds numbers provided the effective adverse pressure gradient at the trailing edge, which is related to the aerofoil thickness distribution, is sufficiently large. For smaller adverse pressure gradients, there exists a critical Reynolds number above which the flow is globally linearly unstable, but below which it is globally stable. An asymptotic analysis for large wavenumber indicates that the double Blasius profile, corresponding to a zero adverse pressure gradient, may be absolutely unstable.

1. Introduction

The problem of wake-flow instability behind a flat plate has been treated many times, with a variety of analytical and numerical techniques. Previously, some attempts have been made to model the behaviour using convenient analytical profiles (Mattingly & Criminale 1972), for example the Gaussian or sech^2 wake, and this approach can often give quite accurate results, particularly for relatively thick plates with blunt trailing edges. However, in the case of a thin aerofoil in zero or small adverse pressure gradients, the qualitative instability characteristics are very sensitive to the exact shape of the velocity profiles close to the trailing edge, and the stability analysis should be performed on the correct wake profiles. This was recognized by Papageorgiou & Smith (1989), who solved the temporal and spatial linear instability problems for the flat-plate case, both numerically for order-one growth rates and using asymptotic analysis for the small- and large-wavenumber cases. As they point out, "...a combined stability problem involving both complex frequency and wavenumber is in principle possible." Their results correspond closely with the experimental results of, amongst others, Sato & Kuriki (1961) and Mattingly & Criminale (1972). In both these experiments the instability was forced by loudspeaker excitation of the flow and, given the presence of the sharp trailing, the spatial analysis of Papageorgiou & Smith (1989) is clearly appropriate.

In order to investigate unforced, or self-excited, oscillations, we must turn instead to the theory of absolute instability and global modes, as discussed by, for example, Monkewitz, Huerre & Chomaz (1993, from here on referred to as MHC93) and Huerre & Monkewitz (1990). Here we attempt to solve the *unforced* instability problem for an aerofoil wake by studying the temporal and spatial evolution of

https://doi.org/10.1017/S0022112097005314 Published online by Cambridge University Press

a delta-function perturbation to the original steady flow. We thus hope to discover whether an initial perturbation to the flow decays, leaving the flow in its original state, or grows exponentially, leading to eventual nonlinear evolution of the perturbation, and a global change in the structure of the flow to Kármán vortex shedding.

Following MHC93 we formulate the problem as a streamwise eigenvalue problem using a multiple-scales-type WKBJ analysis, assuming the flow to be slowly varying in the streamwise direction. Application of a suitable expansion in the small parameter $\epsilon = 1/Re^{1/2}$, with Re the Reynolds number based on aerofoil chord, then allows us to solve a succession of ordinary differential equations and find an asymptotic expression for the global mode frequency and growth rate. We use as the basic state flow both an analogue of the Goldstein (1930) wake (in which we suppose that the flow at the trailing edge is a Falkner–Skan flow with negative pressure gradient) and the genuine aerofoil wake obtained by integration of the boundary layer equations.

We start in §2 by performing the WKBJ analysis of the wake flow, and go on to present the calculation of the specific steady flows under consideration in §3. We describe our numerical results in §4, where we show that for both the aerofoil and the Falkner–Skan profiles there exists a critical Reynolds number for global instability, the value of which depends on the aerofoil thickness or pressure gradient. We also describe a large-wavenumber expansion, which suggests that the double Blasius wake profile may be locally absolutely unstable. Finally, we discuss the relevance of these results to the physical problem at hand and make suggestions for further work on this subject in §5.

2. Analytical results

2.1. *Outer-scale analysis*

We consider a thin uncambered aerofoil of chord length c^* (the superscript denotes dimensional quantities), lying in a two-dimensional incompressible viscous fluid of kinematic viscosity ν^*, with a steady uniform flow of speed U^*_∞ at infinity aligned parallel to the aerofoil chord – see figure 1. Axes with origin at the aerofoil trailing edge are introduced as shown, and the precise form of the aerofoil thickness distribution will be described later. The Reynolds number based on the chord is

$$Re = U^*_\infty c^*/\nu^*, \tag{2.1}$$

and we define the characteristic trailing-edge boundary layer thickness

$$\delta^*_{TE} = c^*\, Re^{-1/2}. \tag{2.2}$$

All physical variables are now non-dimensionalized – lengths by δ^*_{TE}, velocities by U^*_∞ and pressures by $\rho^*_\infty U^{*\,2}_\infty$, where ρ^*_∞ is the fluid density – and in what follows non-dimensional quantities are unstarred. Our susbsequent analysis will be completed in the limit of large Reynolds number, and to facilitate this we introduce the small parameter

$$\epsilon = Re^{-1/2}, \tag{2.3}$$

and consider the asymptotic limit $\epsilon \ll 1$. In this limit, the steady flow past the aerofoil will vary slowly in the streamwise direction (i.e. it is weakly non-parallel), and will therefore depend on streamwise position only in terms of the 'slow' coordinate $X = \epsilon x$, so that when a small unsteady perturbation is introduced on top of the steady flow

https://doi.org/10.1017/S0022112097005314 Published online by Cambridge University Press

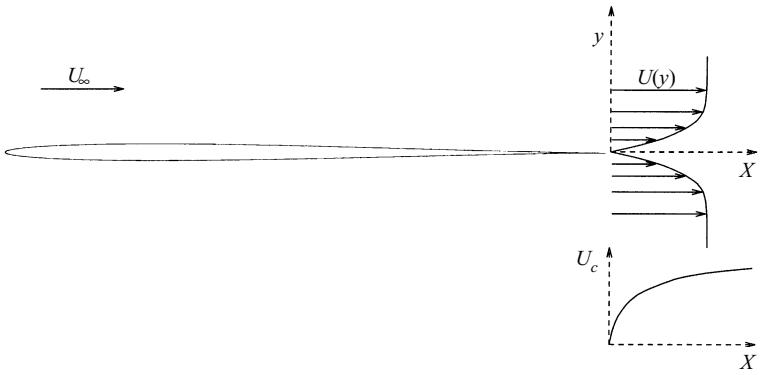

FIGURE 1. Thin aerofoil in uniform stream, also showing the approximate behaviour of the wake centreline velocity $U_c(X)$.

we can write the total fluid velocity $\boldsymbol{u}$ as

$$\boldsymbol{u} = \left(U(y;X) + \frac{\partial \psi'}{\partial y}, V(y;X) - \frac{\partial \psi'}{\partial x} \right). \tag{2.4}$$

Here, $\psi'(x,y,t)$ is the streamfunction of the unsteady perturbation and (U,V) is the steady velocity.

Equation (2.4) is subsituted into the unsteady Navier–Stokes equations, and by linearizing in the perturbation amplitude and eliminating the unsteady perturbation pressure we obtain the evolution equation for ψ' in the form

$$\left[\left(\frac{\partial}{\partial t} + U \frac{\partial}{\partial x} \right) \nabla^2 - \frac{\partial^2 U}{\partial y^2} \frac{\partial}{\partial x} \right] \psi' + O\left(\epsilon^2 |\psi'|, |\psi'|^2 \right) = 0. \tag{2.5}$$

Following MHC93 the idea now is to look for the Green function, $G(x,y,t)$, of (2.5) by introducing the non-zero right-hand side $Q\delta(X - X_s)$, corresponding to a source located on the wake centreline at the point X_s. In fact, we will be attempting to determine the long-time behaviour of $G(x,y,t)$, which as we shall see is typically dominated by a single global mode of frequency ω_G. We first take the time Fourier transform of (2.5), with

$$\hat{G}(x,y,\omega) = \int_{-\infty}^{\infty} G(x,y,t)\, \mathrm{e}^{\mathrm{i}\omega t} \mathrm{d}t, \tag{2.6}$$

and then introduce the standard WKBJ approximation for the Green function,

$$\hat{G}^{\pm} \sim \left[\hat{G}_0^{\pm} + \epsilon \hat{G}_1^{\pm} + O\left(\epsilon^2\right) \right] \exp\left[\frac{\mathrm{i}}{\epsilon} \int_{X^s}^{X} k^{\pm}\left(X';\omega\right) \mathrm{d}X' \right], \tag{2.7}$$

where the $^{\pm}$ denote the solution upstream or downstream of the source; note that $k^{\pm}$ will correspond to the k eigenvalues originating from the upper or lower half-planes respectively. In order to evaluate the asymptotic expansion of $\hat{G}^{\pm}$ we use the method of multiple scales; by introducing the chain rule relation

$$\frac{\partial}{\partial x} \rightarrow \frac{\partial}{\partial x} + \epsilon \frac{\partial}{\partial X} \tag{2.8}$$

into (2.5), and then subsituting for $\hat{G}^{\pm}$ from (2.7) we obtain an ordinary differential equation to solve at each order in ϵ, as is described below.

https://doi.org/10.1017/S0022112097005314 Published online by Cambridge University Press

At $O(\epsilon^0)$ we find that $\hat{G}_0$ must satisfy the Rayleigh equation

$$\mathscr{L}^{\pm}\left\{\hat{G}_0^{\pm}\right\} = 0, \tag{2.9}$$

$$\mathscr{L}^{\pm}\{\cdot\} \equiv \left[\left(k^{\pm}U(y;X)-\omega\right)\left(\frac{\partial^2}{\partial y^2}-k^{\pm 2}\right)-k^{\pm}\frac{\partial^2 U}{\partial y^2}\right]\{\cdot\}, \tag{2.10}$$

the solution of which is

$$\hat{G}_0^{\pm}(y,X) = \bar{A}_0^{\pm}(X)\,\phi_0^{\pm}(y;X), \tag{2.11}$$

where $\phi_0^{\pm}(y;X)$ satisfies the Rayleigh equation at each fixed X. The slowly-varying amplitude function $\bar{A}_0^{\pm}(X)$ should be determined at next order in ϵ by a secularity condition which must be satisfied in order to ensure a uniformly bounded solution for G. However, if the ω-contour in the time inversion of $\hat{G}$ has to be deformed past a branch-point singularity in the ω-plane, where the group velocity $\partial\omega/\partial k = 0$, then it will turn out that this secularity equation breaks down. For the absolutely unstable wake profiles considered this indeed happens, and to avoid this a second scaling in X must be introduced as described below.

2.2. *Rescaling*

The multiple-scales analysis described above yields at $O(\epsilon)$ the secularity condition

$$\frac{\partial\omega}{\partial k}^{\pm}\frac{\mathrm{d}\bar{A}_0^{\pm}}{\mathrm{d}X} = -\left[\frac{1}{2}\mathrm{d}_{kk}^{\pm}\frac{\partial k^{\pm}}{\partial X}+\mathrm{d}_{k\omega}^{\pm}\frac{\partial\omega^{\pm}}{\partial X}\right]\bar{A}_0^{\pm}, \tag{2.12}$$

which is very similar to equation (3.8) of MHC93, the differences being due to our definition of the expansion parameter as $\epsilon = Re^{-1/2}$, compared to $\epsilon = 1/Re$ in their paper. Here we retain as far as possible the same notation as MHC93, in which the $\mathrm{d}_{\dagger}$ represent ratios of inner products introduced by the secularity condition. We shall define d_{kk} fully later on, while $\mathrm{d}_{k\omega}$, which we do not actually need for our problem, can be defined in a similar way. As mentioned above, (2.12) clearly becomes singular when $\partial\omega/\partial k(k,X)$ is zero, and for the purposes of this analysis we shall suppose that this occurs at the single streamwise position X^t, with corresponding frequency and wavenumber ω^t and k^t respectively. The idea now is to introduce an inner scaling to remove this singularity, and in order to do this we first expand the group velocity about (k^t, X^t) as

$$\frac{\partial\omega}{\partial k}(k,X) = \frac{\partial\omega}{\partial k}(k^t,X^t)+(k-k^t)\frac{\partial^2\omega}{\partial k^2}(k^t,X^t)+(X-X^t)\frac{\partial^2\omega}{\partial X\partial k}(k^t,X^t)+\ldots. \tag{2.13}$$

The point at which $\partial\omega/\partial k$ vanishes corresponds to a saddle point in the complex k-plane, in the neighbourhood of which $\omega-\omega^t \sim (k-k^t)^2$, and hence the scalings of the X derivatives of ω and k are given to leading order by the expressions

$$\frac{\partial\omega}{\partial X} \sim \frac{\omega-\omega^t}{X-X^t} \tag{2.14}$$

$$\frac{\partial k}{\partial X} \sim \frac{(\omega-\omega^t)^{1/2}}{X-X^t}, \tag{2.15}$$

and also, due to the dependence on the slow length scale,

$$(k-k^t)(X-X^t) \sim \epsilon. \tag{2.16}$$

https://doi.org/10.1017/S0022112097005314 Published online by Cambridge University Press

Clearly (2.14) and (2.15) indicate that the right-hand side of (2.12) is dominated by the $\partial k/\partial X$ term, since $(\omega-\omega^t)^{1/2}$ is small. Also, for X close to X^t, the left-hand side of (2.12) is dominated by the $(k-k^t)\partial^2\omega/\partial k^2$ term in (2.13), since $(X-X^t)$ is small, and the equation reduces to

$$\left(k-k^t\right)\frac{\mathrm{d}A_0}{\mathrm{d}X}\sim\frac{\left(\omega-\omega^t\right)^{1/2}}{X-X^t}A_0, \tag{2.17}$$

which, on substituting the scaling equation (2.16), becomes

$$\frac{\epsilon}{X-X^t}\frac{1}{X-X^t}\sim\frac{\left(\omega-\omega^t\right)^{1/2}}{X-X^t}, \tag{2.18}$$

and hence

$$X-X^t\sim\frac{\epsilon}{\left(\omega-\omega^t\right)^{1/2}}. \tag{2.19}$$

For the aerofoil wake it will turn out that the turning point X^t is at the trailing edge, so that in fact $X^t=0$, but for the sake of generality we will keep X^t in our analysis explicitly. In this region the basic-state flow will be given by the modified Goldstein wake solution, in which the centreline velocity U_c is proportional to $X^{1/3}$ to leading order in X. It can be shown that for a wide range of wake profiles (Woodley & Peake 1997) the frequency varies approximately linearly with U_c, and we shall show that this is indeed true for our specific case in §4. Hence it follows that

$$\omega-\omega^t\sim\left(X-X^t\right)^{1/3}. \tag{2.20}$$

Equations (2.19) and (2.20) can now be combined, and suggest that we should introduce the inner variable

$$\tilde{X}=\epsilon^{-6/7}\left(X-X^t\right) \tag{2.21}$$

around the turning point, and this will be described in the next subsection.

2.3. *Turning point analysis*

In the light of the rescaling argument given above, we expand the flow variables about $X=X^t$ in the form

$$\left.\begin{aligned} U(y;X)&=U_0(y;X)+\epsilon^{2/7}\tilde{X}^{1/3}U_1(y;X)+O(\epsilon^{3/7}),\\ \psi'&=\left[\bar{\Phi}_0+\epsilon^{1/7}\bar{\Phi}_1+\epsilon^{2/7}\bar{\Phi}_2+O\left(\epsilon^{3/7}\right)\right]\left(\tilde{X},y\right)\times\exp\left\{\frac{\mathrm{i}}{\epsilon}k_0^t\left(X-X^t\right)-\mathrm{i}\omega_G t\right\},\\ \omega_G&=\omega_0^t+\epsilon^{1/7}\bar{\omega}_1+\epsilon^{2/7}\bar{\omega}_2+O\left(\epsilon^{3/7}\right), \end{aligned}\right\} \tag{2.22}$$

where we have replaced the general source location X^s with the turning point X^t. The form of the expansion of the steady flow follows exactly from Goldstein's wake solution – the first term $U_0(y;X)$ is simply the velocity profile at the trailing edge, and the second term includes the $X^{1/3}$ dependence of the Goldstein solution. The new form of the perturbation streamfunction follows directly from the expansion of (2.7) about $X=X^t$, and in particular the linear factor in the exponential arises from the expansion of the WKBJ phase function.

The frequency ω_G is the (unknown) global-mode frequency, which will be determined as part of our solution. The first term in ω_G is the absolute instability frequency of the steady wake profile at X^t, and represents the long-time limit behaviour of a parallel flow $U(y;X^t)$, with the higher-order terms representing corrections to this to

https://doi.org/10.1017/S0022112097005314 Published online by Cambridge University Press

allow for the non-parallel nature of the flow. This first term arises due to the need to deform the WKBJ integration contour through the turning point in the complex X-plane, which in our case is a turning point with $\partial\omega/\partial X \neq 0$, i.e. a boundary contribution, since $X^t = 0$. This point is more fully described in MHC93, and of course follows from the fact that at $O(\epsilon^0)$ the wake flow is strictly parallel, so that the long-time limit of its response corresponds exactly to that of the profile at $X = X^t$, which, for the absolutely unstable profiles considered, is given by the local absolute instability. In fact, we can define a local absolute instability frequency at each X, say $\omega_0(X)$, simply by finding the appropriate branch point of the parallel-flow dispersion relation at X (for a very full description see Huerre & Monkewitz 1990), so that $\omega_0^t = \omega_0(X^t)$. It will be seen later that $\mathrm{Im}[\omega_0(X)] > 0$ for a finite range of $X \geqslant 0$ in our aerofoil wake, corresponding to a pocket of locally absolutely unstable flow; whether or not this leads to a globally unstable flow (i.e. $\mathrm{Im}[\omega_G] > 0$) depends on the correction terms $\bar{\omega}_{1,2}$, and this will be discussed later.

Equation (2.22) is susbtituted into (2.5) as before, and now using the chain rule relation

$$\frac{\partial}{\partial x} \rightarrow \frac{\partial}{\partial x} + \epsilon^{1/7} \frac{\partial}{\partial \tilde{X}} \tag{2.23}$$

and equating powers of ϵ, we find that at $O(\epsilon^0)$ we have the equation

$$\left[\left(-\mathrm{i}\omega_0^t + \mathrm{i}U_0 \frac{\partial}{\partial x}\right)\left(\frac{\partial^2}{\partial y^2} - k^2\right) - \frac{\partial^2 U_0}{\partial y^2}\frac{\partial}{\partial x}\right]\bar{\Phi}_0 = 0, \tag{2.24}$$

and so recover the standard Rayleigh equation

$$\mathscr{L}^t\left\{\phi_0^t\right\} = 0, \tag{2.25}$$

where superscripts ^{t} denote evaluation at the turning point X^t. Thus $\bar{\Phi}_0$ is given by

$$\bar{\Phi}_0\left(\tilde{X}, y\right) = \bar{A}_0\left(\tilde{X}\right)\phi_0^t(y), \tag{2.26}$$

where $\bar{A}_0\left(\tilde{X}\right)$ is a slowly varying amplitude function which must be determined at higher order.

At $O(\epsilon^{1/7})$ we obtain

$$\mathscr{L}^t\left\{\bar{\Phi}_1\right\} = \mathrm{i}\mathscr{L}_k^t\left\{\phi_0^t\right\}\frac{\mathrm{d}\bar{A}_0}{\mathrm{d}\tilde{X}} - \bar{\omega}_1\mathscr{L}_\omega^t\left\{\phi_0^t\right\}\bar{A}_0, \tag{2.27}$$

where the subscripts on the $\mathscr{L}^t$ denote partial differentiation of the operator defined by (2.10) with respect to the subscripted variable (explicit expressions for these operators are given in MHC93). We now take the inner product of (2.27) with the homogeneous solution of the adjoint Rayleigh equation, and obtain the solvability condition

$$\frac{\mathrm{i}\mathrm{L}_k^t\left\{\phi_0^t\right\}}{\mathrm{L}_\omega^t\left\{\phi_0^t\right\}}\frac{\mathrm{d}\bar{A}_0}{\mathrm{d}\tilde{X}} - \bar{\omega}_1\bar{A}_0 = 0, \tag{2.28}$$

where the operator L is defined by

$$\mathrm{L}\left\{\cdot; k, \omega, X\right\} \equiv \int_0^\infty \mathscr{L}\left\{\cdot; k, \omega, X\right\}\frac{\phi_0(y; X)}{kU(y; X) - \omega}\mathrm{d}y, \tag{2.29}$$

and the subscripts on the L in (2.28) again denote differentiation with respect to the subscripted variable. We note that it can be shown (see Appendix A of MHC93) that

$$\frac{\partial\omega}{\partial k} + \frac{\mathrm{L}_k\left\{\phi_0\right\}}{\mathrm{L}_\omega\left\{\phi_0\right\}} = 0, \tag{2.30}$$

https://doi.org/10.1017/S0022112097005314 Published online by Cambridge University Press

and evaluating (2.30) at the turning point X^t where $\partial\omega/\partial k = 0$ and substituting into (2.28), we find that

$$\bar{\omega}_1 = 0. \tag{2.31}$$

The leading-order non-parallel correction to the global mode frequency is therefore identically zero. Returning to (2.27), we now see that

$$\bar{\Phi}_1 = \bar{A}_1\left(\tilde{X}\right)\phi_0^t(y) + \mathrm{i}\frac{\mathrm{d}\bar{A}_0}{\mathrm{d}\tilde{X}}\phi_{1k}^t(y), \tag{2.32}$$

where $\bar{A}_1(\tilde{X})$ is an unknown amplitude function and $\phi_{1k}^t(y)$ is a solution of the inhomogeneous Rayleigh equation

$$\mathscr{L}^t(\phi) = \mathscr{L}_k^t\left(\phi_0^t\right). \tag{2.33}$$

To find the slowly varying amplitude function $\bar{A}_0(\tilde{X})$ we need to go to $O(\epsilon^{2/7})$, where we obtain the equation

$$\begin{aligned}\mathscr{L}^t\left\{\bar{\Phi}_2\right\} = \mathrm{i}\mathscr{L}_k^t\left\{\phi_0^t\right\}\frac{\mathrm{d}\bar{A}_1}{\mathrm{d}\tilde{X}} - \left[\mathscr{L}_k^t\left\{\phi_{1k}^t\right\} - \tfrac{1}{2}\mathscr{L}_{kk}^t\left\{\phi_0^t\right\}\right]\frac{\mathrm{d}^2\bar{A}_0}{\mathrm{d}\tilde{X}^2} \\ - \left[\bar{\omega}_2\mathscr{L}_\omega^t\left\{\phi_0^t\right\} + \tilde{X}^{1/3}\mathscr{L}_X^{1t}\left\{\phi_0^t\right\}\right]\bar{A}_0,\end{aligned} \tag{2.34}$$

where we have introduced a new operator $\mathscr{L}_X^1$ that represents the analogue of the X-derivative Rayleigh operator, defined as

$$\mathscr{L}_X^1\{\cdot;k,\omega,X\} = \left[kU_1\left(\frac{\partial^2}{\partial y^2} - k^2\right) - kU_{1yy}\right]\{\cdot;k,\omega,X\}. \tag{2.35}$$

Taking the inner product of (2.34) as before and dividing through by $\mathrm{L}_\omega\{\phi_0^t\}$, we now obtain the modified secularity condition

$$\frac{\mathrm{i}\mathrm{L}_k^t\left\{\phi_0^t\right\}}{\mathrm{L}_\omega^t\left\{\phi_0^t\right\}}\frac{\mathrm{d}\bar{A}_1}{\mathrm{d}\tilde{X}} - \frac{1}{2}\mathrm{d}_{kk}^t\frac{\mathrm{d}^2\bar{A}_0}{\mathrm{d}\tilde{X}^2} - \left[\bar{\omega}_2 - \mathrm{d}_X^{1t}\tilde{X}^{1/3}\right]\bar{A}_0 = 0, \tag{2.36}$$

where d_X^{1t} is given by

$$\mathrm{d}_X^{1t} = -\frac{\mathrm{L}_X^{1t}\left\{\phi_0^t\right\}}{\mathrm{L}_\omega^t\left\{\phi_0^t\right\}}, \tag{2.37}$$

and

$$\mathrm{d}_{kk}^t = \frac{2\mathrm{L}_k^t\left(\phi_{1k}^t\right) - \mathrm{L}_{kk}^t\left(\phi_0^t\right)}{\mathrm{L}_\omega^t\left(\phi_0^t\right)}. \tag{2.38}$$

It can then easily be shown, using the above definition of L_ω^t and the fact that ϕ_0^t must satisfy the Rayleigh equation (2.10), that

$$\mathrm{L}_\omega^t\left\{\phi_0^t\right\} = -k\int_0^\infty \frac{U_{yy}\left(\phi_0^t\right)^2}{kU-\omega}\mathrm{d}y, \tag{2.39}$$

which on substitution into (2.37) above gives

$$\mathrm{d}_X^{1t} = \frac{\displaystyle\int_0^\infty\left[\frac{kU_1U_{yy}}{kU-\omega} - U_{1yy}\right]\frac{\left(\phi_0^t\right)^2}{kU-\omega}\mathrm{d}y}{\displaystyle\int_0^\infty\frac{U_{yy}\left(\phi_0^t\right)^2}{kU-\omega}\mathrm{d}y}. \tag{2.40}$$

https://doi.org/10.1017/S0022112097005314 Published online by Cambridge University Press

Now applying the condition that the complex group velocity $\partial\omega/\partial k$ is zero at X^t in (2.30), we see that the term involving $\bar{A}_1$ in the secularity condition (2.36) vanishes, so that the secularity condition reduces to an ordinary differential equation for the unknown amplitude $\bar{A}_0$ in the form

$$\frac{\mathrm{d}^2\bar{A}_0}{\mathrm{d}\tilde{X}^2} + \frac{2\left(\bar{\omega}_2 - \mathrm{d}_X^{1t}\tilde{X}^{1/3}\right)}{\mathrm{d}_{kk}^t}\bar{A}_0 = 0. \tag{2.41}$$

Finally, it proves convenient to introduce into (2.41) a rescaling of the form

$$u = \left(\frac{2\mathrm{d}_X^{1t}}{\mathrm{d}_{kk}^t}\right)^{3/7}\tilde{X}, \tag{2.42}$$

to give the 'Airy-like' equation

$$\frac{\mathrm{d}^2\bar{A}_0}{\mathrm{d}u^2} + \left(a - u^{1/3}\right)\bar{A}_0 = 0, \tag{2.43}$$

where a is given by

$$a = \frac{2\bar{\omega}_2}{\mathrm{d}_{kk}^t}\left(\frac{2\mathrm{d}_X^{1t}}{\mathrm{d}_{kk}^t}\right)^{-6/7}. \tag{2.44}$$

The boundary conditions for (2.41) are

$$\bar{A}_0\,(u = \infty) = 0 \tag{2.45}$$

$$\bar{A}_0\left(u = -\left(\frac{2\mathrm{d}_X^{1t}}{\mathrm{d}_{kk}^t}\right)^{3/7}\epsilon^{-6/7}X^t\right) = 0, \tag{2.46}$$

and correspond to the requirement that the mode amplitude is zero at the trailing edge $X = 0$ and at downstream infinity. The former condition is the unsteady Kutta condition, requiring that the normal velocity is zero at the trailing edge, $X = 0$, and hence that $\bar{A}_0(0) = 0$. This condition may also be interpreted in terms of the assumption that the aerofoil has no effect on the development of the global mode other than in setting up the steady wake profiles – this is the usual approach taken in wake stability problems, and is supported by the numerical evidence of Triantafyllou & Karniadakis (1990). The branch cut in (2.42) is chosen so that the integration contour along the real X-axis can be deformed into the complex u-plane without changing the asymptotic behaviour at infinity, and by defining the branch cuts as in the Appendix we obtain a self-consistent way of performing transformation (2.42), which finally results in a unique definition of $\bar{\omega}_2$.

For our problem, we note that the trailing-edge profile has a k saddle point, and hence the turning point is actually *at* the trailing edge, i.e. $X^t = 0$. Our results showed no indication of any other turning points on the streamwise axis; one would expect this due to the monotonic increase of the centreline velocity, and corresponding decrease of the locally parallel growth rate, downstream of the trailing edge. Hence the boundary conditions reduce to

$$\bar{A}_0\,(u = \infty) = 0, \tag{2.47}$$

$$\bar{A}_0\,(u = 0) = 0. \tag{2.48}$$

Equations (2.43), (2.47) and (2.48) thereby define an eigenvalue problem for a which can be solved to determine the correction $\bar{\omega}_2$ to the global mode frequency. This

https://doi.org/10.1017/S0022112097005314 Published online by Cambridge University Press

correction depends on the precise form of the steady wake in the neighbourhood of the trailing edge through terms such as $\mathrm{d}_X^{1t}/\mathrm{d}_{kk}^{t}$ in (2.42), and in the next section we will proceed to calculate $\bar{\omega}_2$ for our aerofoil wake. We note here, however, that no inference about the sign of $\mathrm{Im}[\bar{\omega}_2]$ can be made at this stage, and indeed it will turn out that both stabilizing and destabilizing non-parallel corrections are possible, depending on the aerofoil thickness.

3. Basic-state flow

3.1. *Outer flow and aerofoil boundary layer calculation*

For definiteness we suppose that the aerofoil is an uncambered Zhukovski aerofoil, although it should be emphasized that any standard thickness distribution could equally well be used. The inviscid flow past a Zhukovski aerofoil lying in the complex z-plane is well known, and can be found by applying the transformation

$$z = \zeta + a^2/\zeta \tag{3.1}$$

to the cylinder $|\zeta + b| = a + b$ in the ζ-plane (Acheson 1990). For thin aerofoils it follows that a is approximately equal to the quarter-chord length, giving the maximum aerofoil thickness to chord ratio of $t = 3\sqrt{3}b/4a$. This outer inviscid flow provides the slip velocity on the aerofoil surface, and hence to find the boundary layer flow we integrate the boundary layer equations downstream from the leading-edge stagnation point, with the inviscid slip velocity calculated above as the outer boundary condition, using a Crank–Nicholson method described in Panton (1984). The solution for the steady boundary layer flow will of course not remain valid if the flow separates; we were therefore careful to test for separation at each step in the downstream marching, and found that the flow remains attached all the way to the trailing edge provided $b/a \leqslant 0.0351$, corresponding to a thickness to chord ratio of around 4.5%. It should also be noted that, since the Zhukovski aerofoil has a cusped trailing edge, the flow does not then separate at the trailing edge either.

3.2. *Wake-flow calculation*

Once we have calculated the steady boundary layer profile at the trailing edge, we must then 'march' the solution downstream of the trailing edge to find the steady wake flow. This was done using the method formulated by Smith (1974) for handling the discontinuity in boundary conditions at the aerofoil trailing edge, which is fully described in the context of wake flow by Daniels (1976), and only the briefest explanation is required here. We introduce the new streamwise coordinate $\xi = X^{1/3}$, to fit in with the anticipated scaling of the wake close to the trailing edge as described by Goldstein (1930), and since the aerofoil is uncambered and symmetric we restrict attention to the region $y \geqslant 0$. We then split the wake into two regions – an inner region (I) in which $y = O(\xi)$, with grid points spaced evenly in ξ and y/ξ, and an outer region (II), for $y = O(1)$, with grid points spaced evenly in ξ and y. In region II the initial condition at $\xi = 0$ is provided by the boundary layer flow at the trailing edge, while at $\xi = 0$ the flow in region I is driven by the trailing-edge shear stress and can be found in terms of a similarity solution (Daniels 1976). The solutions in these two regions are then marched downstream, with the streamfunction and its derivatives matched together at the boundary between regions I and II. At the outer edge of region II we match the streamwise velocity onto the outer wake velocity predicted by the inviscid solution, while on the centreline $y = 0$ we impose zero normal velocity since the steady flow is symmetric. In our calculations we used $\Delta\xi = 0.02$, with the

https://doi.org/10.1017/S0022112097005314 Published online by Cambridge University Press

outer edge of region I at $y/\xi = 5$ with mesh size 0.1, and the outer edge of region II at $y = 10$ with mesh size 0.1. We note here that after each downstream marching step the number of mesh points in region I must be reduced by one, but full details are given in Smith (1974) and Daniels (1976). For $b/a = 0$, i.e. the flat-plate (Blasius boundary layer) case, our numerical solution agreed exactly with the values presented by Daniels (1976).

As a preliminary to analysing the genuine aerofoil wake, we also considered the case in which the boundary layer at $\xi = 0$ has simply a Falkner–Skan profile with negative pressure gradient, which may be representative of the conditions found in aero-engine compressors, an area which provided some of the motivation for this investigation. The streamfunction at $\xi = 0$ is then

$$\frac{U_\infty L}{Re} f\left(\frac{y^*}{L\,Re^{1/2}}\right), \tag{3.2}$$

where $f(\eta)$ satisfies the Falkner–Skan equation

$$f''' + \tfrac{1}{2}(m+1) f f'' + m\left(1 - f'^2\right) = 0. \tag{3.3}$$

We considered negative m in the range $-0.09 \leqslant m < 0$, corresponding to an adverse-pressure-gradient, but unseparated, boundary layer. This profile is then marched downstream from the trailing edge as described above.

4. Numerical method and results

Here we present a range of numerical results obtained by solving the equations presented in §2. In §4.1 we consider the leading-order term ω_0^t in the global mode frequency, as calculated using the locally parallel-flow approximation at $\xi = 0$, while in §4.2 we investigate the effects of the non-parallel correction term $\bar{\omega}_2$. We consider both the genuine aerofoil wake and the Falkner–Skan model wake – it will turn out that the stability properties are qualitatively very similar due to the fact that the trailing-edge profiles obtained by integrating the boundary layer equations all the way from the leading edge are quite well approximated by Falkner–Skan profiles, at least in terms of the position and strength of the inflection points.

The local Rayleigh eigenvalue problem was solved by a straightforward fourth/fifth order Runge–Kutta method, together with a combination of a modified Powell hybrid method (both from the NAG Fortran library) and a complex contour integral method for the root finding. We found that solving the pressure form of the Rayleigh equation, that is

$$p'' - \frac{2U'p'}{U - \omega/k} - k^2 p = 0, \tag{4.1}$$

where $p(y)\exp(\mathrm{i}kx - \mathrm{i}\omega t)$ is the unsteady pressure perturbation, gave better results than solving the streamfunction form (2.10), as it allows us to lower the differentiability requirements on $U(y)$. This is important when the wake is close to the double Blasius profile, for which the stability characteristics are very sensitive to the derivatives of the profile. Of course the eigenvalues of the two formulations are the same, and the resulting pressure eigenfunctions may be easily converted into streamfunction form using the y momentum equation. We also used a contour integral method for the numerical differentiation of ω with respect to k for the saddle point location, which has the advantage of conserving the precision of ω. We found that this method gave good precision with relatively few integration points, provided that the contour did

https://doi.org/10.1017/S0022112097005314 Published online by Cambridge University Press

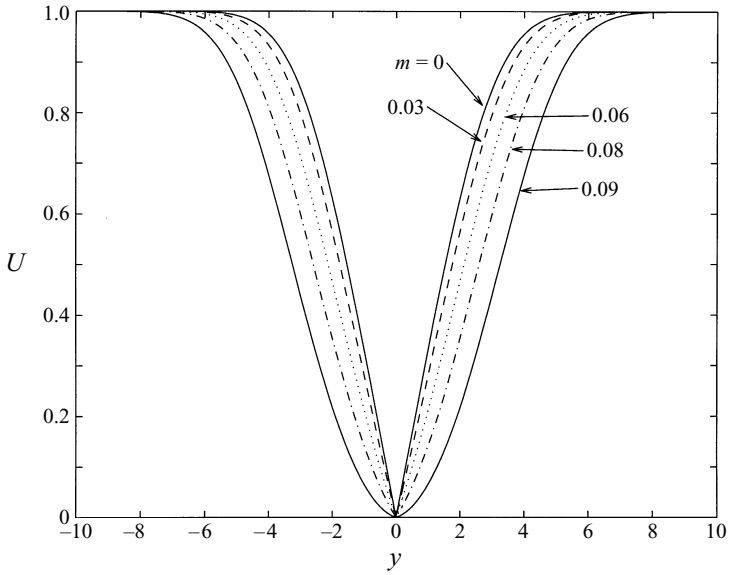

FIGURE 2. Trailing edge ($\xi = 0$) velocity profiles for $m = 0, -0.03, -0.06, -0.08$ and -0.09.

not pass too close to any poles or zeros of the function. We also used a straightforward linear extrapolation procedure to step the parameter, either m (Falkner–Skan profiles) or t (Zhukovski aerofoil profiles) from one profile to the next, which, together with the contour integral methods, allowed rapid location of the saddle points given a suitable guess at the answer for the first profile.

4.1. *Leading-order behaviour*

Figure 2 shows the trailing-edge velocity profiles for a range of the Falkner–Skan pressure gradient parameter, m. We see that the effect of making m less negative is to move the inflection point further in towards the centreline, approaching the non-inflectional double Blasius profile in the limit $m \nearrow 0$, as can be seen more clearly in figure 3 which shows the behaviour of the second derivative of the velocity for three different values of m. Exactly the same behaviour can be observed in the genuine aerofoil profiles, where increasing the aerofoil thickness is equivalent to making m more negative.

We calculated the leading-order eigenvalues, ω_0 and k_0, as described above, but before proceeding one must check that the saddle-point eigenvalue k_0 satisfies the Briggs–Bers (Briggs 1964; Bers 1975, 1983) pinching criterion, in which the two k-roots forming the saddle coalesce from opposite sides of the wavenumber inversion contour as the imaginary part of ω is reduced down to zero, thereby guaranteeing that the solution is causal. A sample contour plot of $\omega(k)$ for the Falkner–Skan profile $\xi = 0$, $m = -0.02$ is shown in figure 4, demonstrating that the two roots do indeed originate from the upper and lower halves of the k-plane as required. It was checked that this remains the case for all the other velocity profiles used.

Figure 5 shows the growth rate behaviour, that is $\omega_{0,i}(X)$, close to the trailing edge. The growth rate appears to be linear in $\xi = X^{1/3}$ close to $\xi = 0$, indicating that the scaling introduced in (2.20) is indeed valid. Note also that there is a pocket of locally absolute instability ($\omega_{0,i} > 0$) in $\xi \geqslant 0$ for $m < 0$, and that the size of this region increases as m becomes more negative; equivalently, the genuine aerofoil

https://doi.org/10.1017/S0022112097005314 Published online by Cambridge University Press

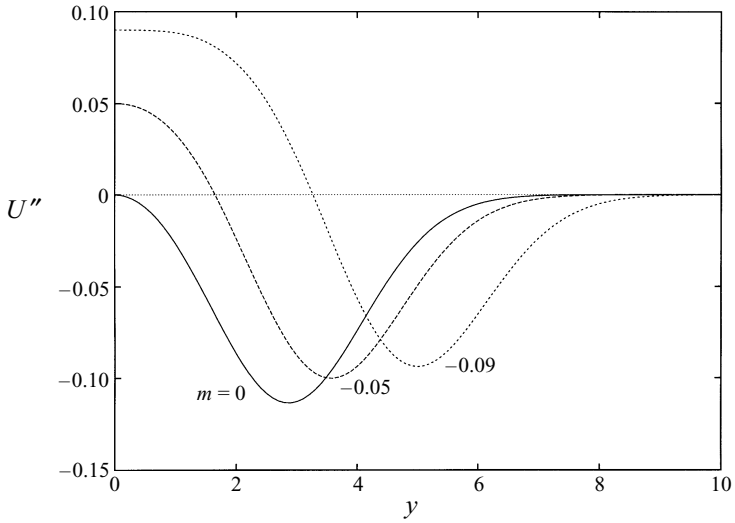

FIGURE 3. Second derivative of velocity against y for $m = 0$, -0.05 and -0.09, showing the position of the inflection point.

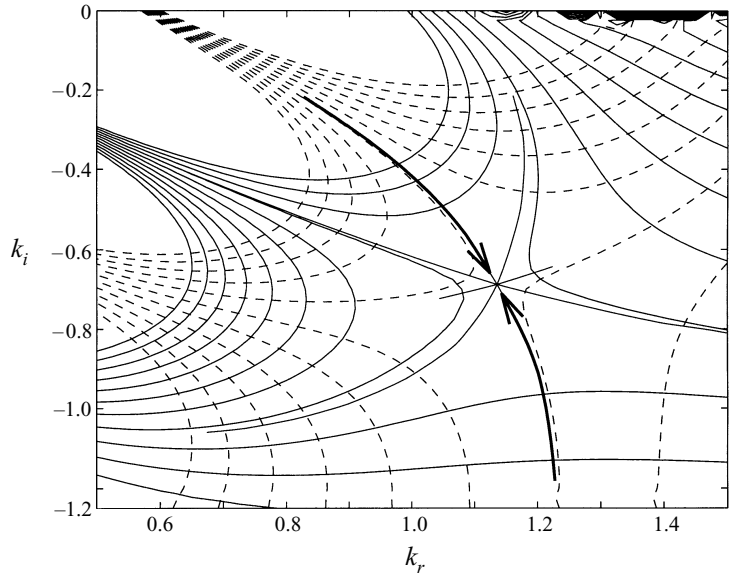

FIGURE 4. Contours of constant $\mathrm{Re}[\omega_0]$ (dashed lines) and $\mathrm{Im}[\omega_0]$ (solid lines) in the complex k-plane for the Falkner–Skan profile $\xi = 0$, $m = -0.02$. Thick arrows denote the locus of the roots $k^{\pm}$ for ω_r constant, $\omega_i \searrow \omega_{0,i}$.

wake has a pocket of absolute instability, the size of which increases with increasing aerofoil thickness. In figures 6 and 7 the local absolute growth rate is plotted against the pressure gradient parameter and thickness ratio respectively for fixed $\xi = 0$. Although these graphs do show that the growth rate decreases significantly as either m or the thickness ratio t approach zero, they also seems to indicate that the growth rate is not actually tending to zero at $m, t = 0$, but we shall return to this point in §5. It was found that for small m or t, the correct saddle point for large ξ was

https://doi.org/10.1017/S0022112097005314 Published online by Cambridge University Press

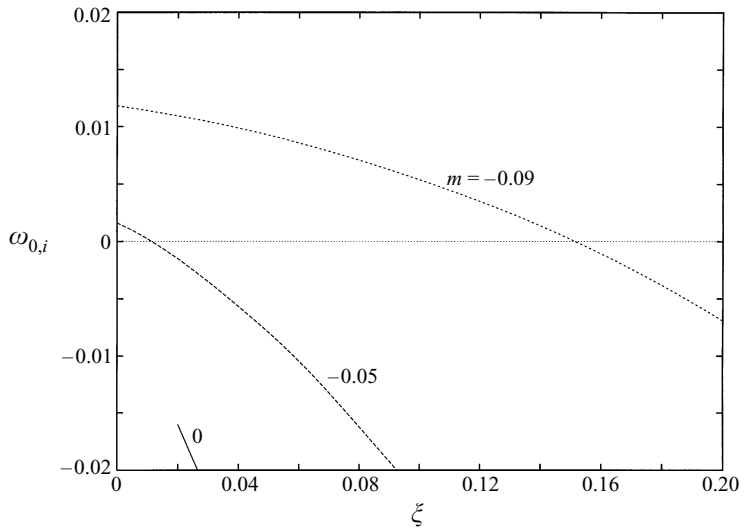

FIGURE 5. Growth rate against downstream distance for $m = 0, -0.05$ and -0.09.

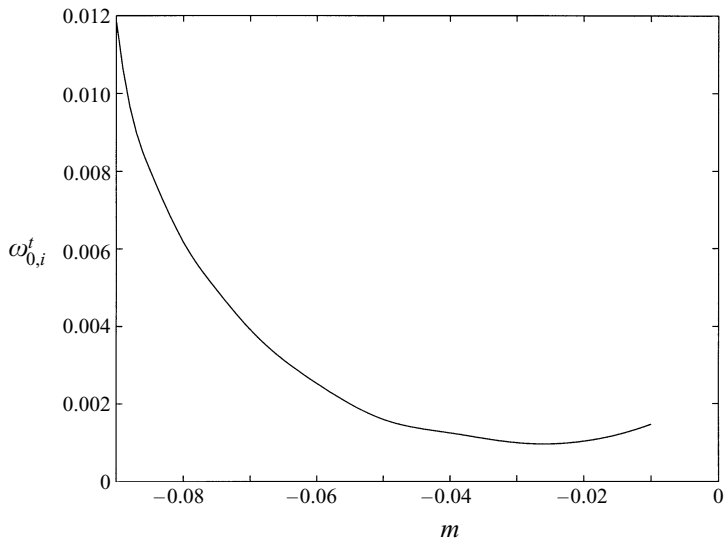

FIGURE 6. Trailing-edge growth rate against pressure gradient parameter, m, for the Falkner–Skan wake.

difficult to find, and we therefore used a parameter stepping procedure using m as the parameter and keeping $\xi = 0$ fixed. Figure 8 shows the locus of the trailing-edge saddle point in the complex wavenumber plane, as m varies from -0.09 to -0.01. It is the rapid variation in the position of k_0 as m approaches zero that causes the problems associated with finding the saddle – this is due to the movement of the inflection point in towards the wake centreline (see figure 3) which causes the eigenfunction to become more localized in the centre of the wake, as indicated in figure 9. Very similar results are obtained for the Zhukovski aerofoil case.

The real part of the global mode frequency for the Falkner-Skan trailing-edge profiles is plotted in figure 10, where it can be seen that the scaled frequency varies

https://doi.org/10.1017/S0022112097005314 Published online by Cambridge University Press

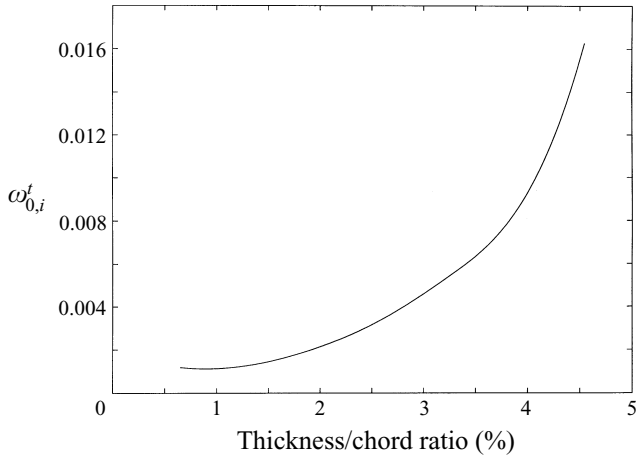

FIGURE 7. Trailing-edge growth rate against thickness ratio, t, for the Zhukovski aerofoil wake.

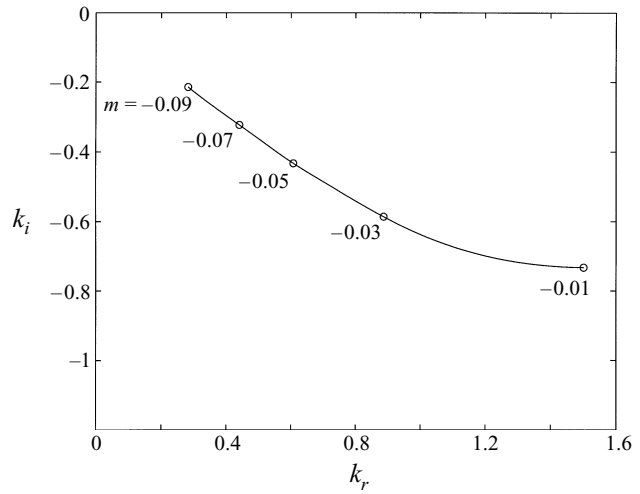

FIGURE 8. Locus of the saddle point k_0 in the complex plane as m tends to zero from below.

only weakly with m. This result could be regarded as quite surprising, given the large effect that the adverse pressure gradient has on the growth rate. However, the real part of the frequency in fact is much more dependent on the overall width of the wake, which remains largely unchanged as m varies, while in contrast the growth rate depends crucially on the shape of the wake near the centreline, which is very sensitive to the value of m.

4.2. *Correction term*

For m in the range $-0.09 < m < 0$, we can calculate the $O(\epsilon^{2/7})$ frequency correction, $\bar{\omega}_2$, from the eigenvalues of the problem defined by (2.43), (2.47) and (2.48). The solutions of this problem, $\bar{A}_0$, are shown in figure 11 for the three smallest eigenvalues – in fact one might expect an infinite spectrum of eigenvalues for a, with a different global mode eigenfunction corresponding to each zero of the 'Airy-like' function. However, in what follows we shall concentrate on only the first mode, which has

https://doi.org/10.1017/S0022112097005314 Published online by Cambridge University Press

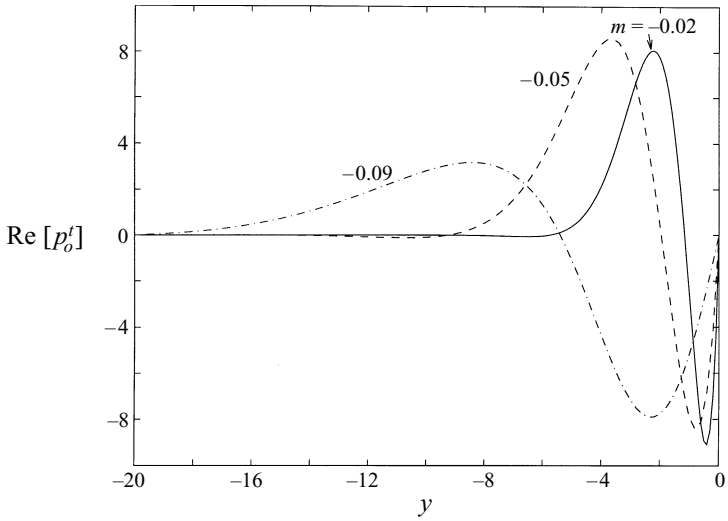

FIGURE 9. Real part of the saddle point eigenfunction Re $\left[p_0^t\right]$ against y for a range of m.

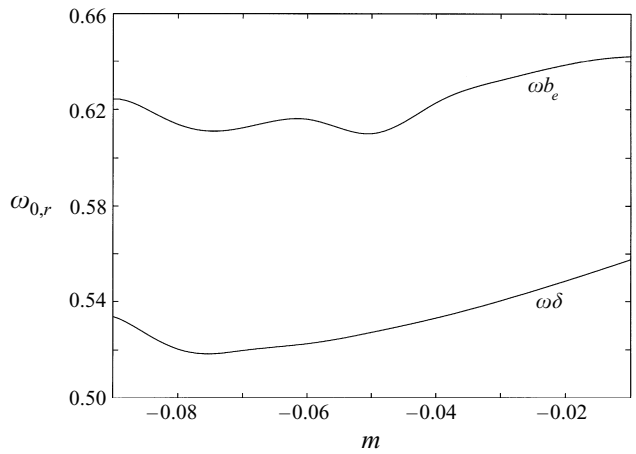

FIGURE 10. Real part of the leading-order global mode frequency, $\omega_{0,r}$ against pressure gradient parameter m, scaled with the wake displacement thickness δ and 1/e-width b_e.

$a = 1.62$, since this mode will give rise to the lowest critical Reynolds number for an instability for any given aerofoil thickness or pressure gradient.

From figure 12 it may be seen that for the Falkner–Skan wake the imaginary part of the frequency correction is positive for m less than some critical value, around -0.035. In this range, the total global mode frequency $\omega_G \sim \omega_0 + \epsilon^{2/7}\bar{\omega}_2$ has a positive imaginary part for all $\epsilon > 0$, and the flow is thus globally unstable for all Reynolds numbers. For $m > -0.035$, however, the frequency correction $\bar{\omega}_2$ has a negative imaginary part and is stabilizing, while the leading-order frequency ω_0 still has a positive imaginary part. In this case we can suggest that there exists a critical value of ϵ, and hence of Re, leading to a neutrally globally stable mode. This critical Reynolds number, for which the imaginary parts of the first two terms balance, is

https://doi.org/10.1017/S0022112097005314 Published online by Cambridge University Press

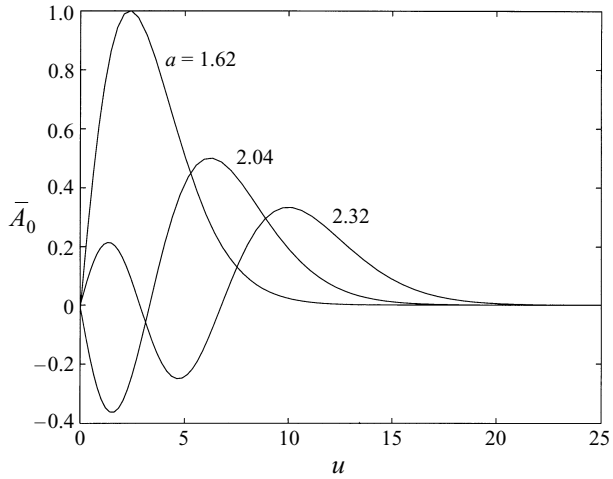

FIGURE 11. Slowly varying amplitude $\bar{A}_0$ as a function of scaled downstream distance u for three values of a. The three amplitudes have been scaled differently for clarity, although of course the actual maximum amplitude is arbitrary in each case.

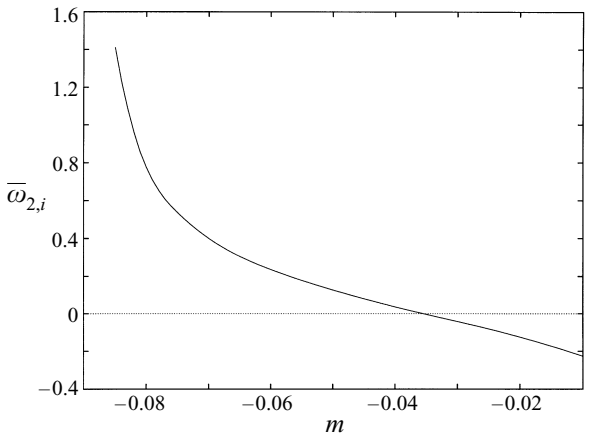

FIGURE 12. Imaginary part of the frequency correction $\bar{\omega}_2$ against pressure gradient parameter m.

given by the expression

$$Re_{crit} = \left(\frac{-\bar{\omega}_{2,i}}{\omega_{0,i}} \right)^7; \tag{4.2}$$

for $Re > Re_{crit}$, the flow is globally unstable, but for $Re < Re_{crit}$ the $O(\epsilon^{2/7})$ correction is large enough to render the flow globally stable. There is extensive experimental evidence (for example Schumm, Berger & Monkewitz 1994) that the wakes of bluff bodies of various aspect ratios undergo such bifurcations to globally unstable modes at sufficiently high Reynolds numbers, although as far as we are aware there is no corresponding evidence for this in thin flat-plate wakes.

It should be noted that the Reynolds number variation has been included only in the sense of changing the non-parallel effect on the correction term; we have not included the viscous effects in the leading order growth rate – for this we would require a full Orr–Sommerfeld analysis for the leading-term. Similarly, it might be

https://doi.org/10.1017/S0022112097005314 Published online by Cambridge University Press

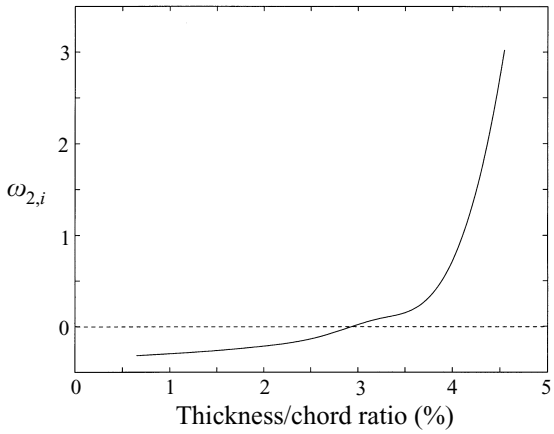

FIGURE 13. Imaginary part of ω_2 against maximum thickness to chord ratio.

expected that the viscous triple-deck region close to the trailing edge would exhibit a strong influence on the stability properties. The effects though are unknown at present, and inclusion of them into the calculation would appear to be a daunting task, due to the non-parallel nature of the flow in this region.

Furthermore, due to the seventh power appearing in (4.2), the critical Reynolds number predicted is very sensitive to the calculation of both the leading-order growth rate, $\omega_{0,\mathrm{i}}$ and the correction growth rate $\bar{\omega}_{2,i}$; hence the predictions can only really be used as order-of-magnitude estimates, given that it is not possible in many cases to calculate $\bar{\omega}_2$ to very high precision. This large power also manifests itself in that relatively large Reynolds numbers are required for ϵ to be reasonably small. Of course, this is an asymptotic theory based on the limit of large Reynolds number, and how small ϵ needs to be to ensure sufficient accuracy of the results is unknown. What we can say, regarding figure 14, is that the critical Reynolds number increases very rapidly for thickness/chord ratios of less than the critical value of around 3%, and hence ϵ is reasonably small at almost all critical Reynolds numbers shown in figure 14. The flow is thus likely to be globally stable for all practical Reynolds numbers provided the thickness/chord ratio is reasonably smaller than the critical value.

The results for the Zhukovski aerofoil are qualitatively the same; the graph of imaginary part of the frequency correction against aerofoil thickness parameter is given in figure 13, along with the corresponding critical Reynolds number plot as defined by (4.2) in figure 14.

4.3. *Large-k asymptotics for the double Blasius wake*

In the limit as $m \nearrow 0$ for the Falkner–Skan wake profiles, or equivalently as $t \searrow 0$ for the Zhukovski aerofoil profiles, the modulus of the turning-point wavenumber increases significantly (figure 8) and the eigenfunction becomes more oscillatory in the centre of the wake (figure 9), causing difficulties in the numerical solution of the Rayleigh equation and subsequent location of the k saddle points. In order to examine this more carefully, we extend Papageorgiou & Smith's (1989) analysis of the asymptotic limit of large k for the spatial stability problem to include the case where both the freqeuncy and wavenumber are complex. To do this, one simply needs to solve the problem treated in Appendix A of their paper, that is solve the boundary layer equations for asymptotically large k in the wake, and only a brief outline need be presented here.

https://doi.org/10.1017/S0022112097005314 Published online by Cambridge University Press

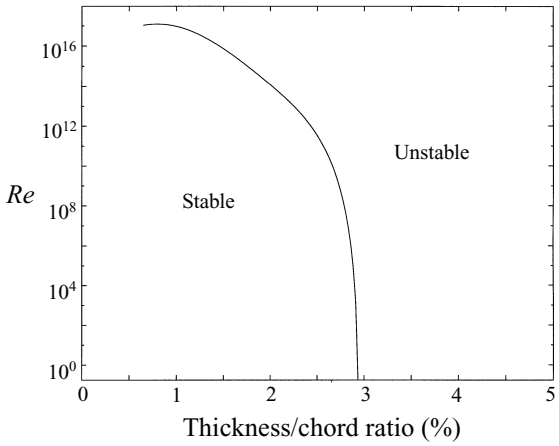

FIGURE 14. Critical Reynolds number against maximum thickness to chord ratio.

Starting from the Rayleigh equation

$$\left(U-\omega/k\right)\left(\psi''-k^2\psi\right)-U''\psi=0, \tag{4.3}$$

we expand the dependent variables in terms of the wavenumber k, with $|k|\gg 1$, as

$$\omega = c_0 k + c_1 + \frac{c_2}{k} + \frac{c_3}{k^2} + \frac{c_4}{k^3} + \ldots, \tag{4.4}$$

$$U = \frac{\lambda Y}{k} + \frac{\lambda_4 Y^4}{k^4} + \ldots, \tag{4.5}$$

$$\psi = \psi_0 + \frac{\psi_1}{k} + \frac{\psi_2}{k^2} + \frac{\psi_3}{k^3} + \ldots, \tag{4.6}$$

where $Y=|k|y$ is the scaled cross-stream coordinate. Here, the coefficients λ and λ_4 are determined from the expansion of the Goldstein wake close to the wake centreline, and are given by Goldstein (1930) as $\lambda\approx 0.332\ldots$ and $\lambda_4=-(1/48)\lambda^2$.

On expanding and solving for successive powers in k, we obtain the results given by Papageorgiou & Smith (1989) for the coefficents in the ω-expansion, that is

$$c_0 = c_2 = c_3 = 0, \tag{4.7}$$

$$c_1 = \lambda, \tag{4.8}$$

$$c_4 = \frac{\lambda}{2A_0}\left[2A_0A_G - 4SI_a + \frac{4\mathrm{i}\pi S}{e^2}\right], \tag{4.9}$$

where A_0 is the amplitude of the leading-order term in the streamfunction expansion $\left(\psi_0 = A_0\mathrm{e}^{-|Y|}\right)$, $S=6\lambda_4A_0/\lambda$, A_G is the (constant) Goldstein displacement thickness and I_a is a definite integral arising from the matching of the streamfunction across the critical layer $Y=1$; we have

$$I_a = \int_0^\infty \frac{W^2\mathrm{e}^{-2W}\,\mathrm{d}W}{W-1}, \tag{4.10}$$

evaluated in a Cauchy principal-value sense.

Using these results, we may now plot the imaginary part of ω against complex k, to show that the double Blasius profile could be absolutely unstable provided the saddle point lies in the correct region of the k-plane, as in figure 15. Overlaying the path of the saddle point, determined numerically, as the profile (either Falkner–Skan or

https://doi.org/10.1017/S0022112097005314 Published online by Cambridge University Press

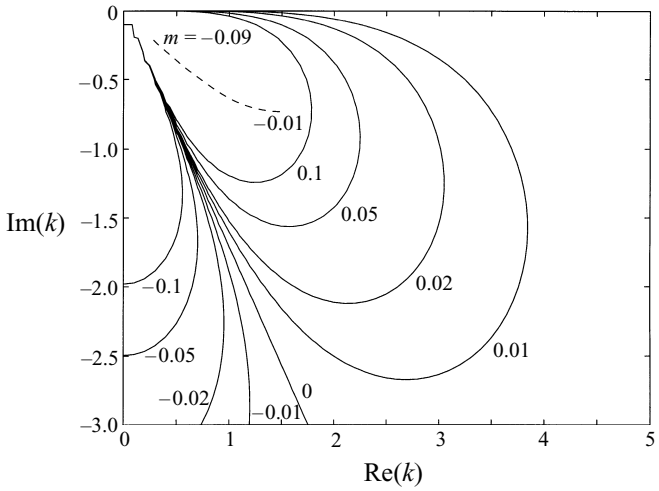

FIGURE 15. Imaginary part of ω for the double Blasius profile over the fourth quadrant of the k-plane, and the locus of the saddle point for varying pressure gradient.

Zhukovski aerofoil type) approaches the double Blasius case, we see that the saddle point is definitely moving in the direction which takes it further into the region where the imaginary part of ω is positive. This also seems to indicate at least qualitative agreement with figures 6 and 7, which show the imaginary part of the leading-order frequency starting to increase as the profiles approach the double Blasius case. Of course, to calculate the position of the saddle point using the large-k asymptotic analysis, we would need to go to at least one more order in k, and we are currently investigating this problem.

5. Concluding remarks

In this paper we have used a multiple-scales-type expansion in the limit of large Reynolds number to determine the long-time limit behaviour of an aerofoil wake. We have determined the global instability frequency to second order in our small expansion parameter $\epsilon^{1/7}$, thus enabling us to calculate the boundaries between different types of long-time behaviour. The results indicate that for a Zhukovski aerofoil the wake is globally unstable to $O(\epsilon^{2/7})$, provided that the maximum thickness/chord ratio, t, is greater than 3%. For each $t < 3\%$, there exists a critical Reynolds number below which the wake is globally stable. Similarly, for the Falkner–Skan wake, the wake stability depends on the adverse-pressure-gradient parameter, m, where again there exists a critical value of $m = -0.035$. For more severe adverse-pressure-gradients the wake is globally unstable for all Reynolds numbers, while for weaker ones there exists a critical Reynolds number below which the flow is globally stable to the asymptotic order calculated here.

One motivation for studying aerofoil wake stability is the phenomenon of acoustic resonance in gas turbine compressor stages, where it is thought that vortex shedding from a poorly performing blade row is a major factor in the occurrence of potentially damaging resonance events. Here we have taken as our model the vortex shedding from both a single flat plate in a flow with an adverse pressure gradient, or, similarly, the wake of a thin Zhoukowski aerofoil in a uniform stream, as a first step towards predicting the vortex-shedding behaviour of such a real system. The model can easily

https://doi.org/10.1017/S0022112097005314 Published online by Cambridge University Press

be extended to the case of a cascade of aerofoils, by using the cascade periodic boundary conditions for the numerical solution of equation (2.9). It can be shown (Woodley & Peake 1997) that the influence of cascade boundary conditions is very small unless the wake thickness is about half the inter-blade spacing, and although this is very unlikely in experimental set-ups of non-rotating cascades, it could easily occur in rotating compressor stages. Similarly, in a real compressor the flow is compressible, and although previous calculations indicate that the compressibility has only a small effect on the local absolute instability properties, the consequences for the correction terms are unclear and are currently under investigation.

In cases where the flow is globally unstable, we expect the oscillation to grow exponentially in time until nonlinear effects become important, at which point this current model breaks down and a weakly nonlinear analysis would be appropriate, in order to determine the frequency shift of the oscillation as it enters the nonlinear regime. At this point, it might also be appropriate to go into the fully nonlinear regime, using a Stuart–Landau model, which has been shown by Schumm *et al.* (1994) to apply very well to vortex shedding behind a body with a blunt trailing edge.

The authors would like to thank Dr S. J. Cowley for helpful conversations and to acknowledge the support of Rolls-Royce plc and the Engineering and Physical Sciences Research Council.

Appendix. Branch cuts in §2

We now consider how to define the branch cuts in the eigenvalue problem at the end of §2. For large $\tilde{X}$, substituting $\bar{A}_0(\tilde{X}) = \exp[\alpha\tilde{X}^{\beta}(1+\ldots)]$ into (2.41) gives

$$\alpha^2\beta^2\tilde{X}^{2(\beta-1)} + \alpha\beta\,(\beta-1)\,\tilde{X}^{\beta-2} - \frac{2\mathrm{d}_X^{1t}}{\mathrm{d}_{kk}^{t}}\tilde{X}^{1/3} = 0\,, \tag{A 1}$$

and comparing powers of $\tilde{X}$ we see that $\beta = \frac{7}{6}$ is the only value that gives a balance in the equation to leading order, and so we get the following equation for the coefficient α:

$$\frac{49}{36}\alpha^2 - \frac{2\mathrm{d}_X^{1t}}{\mathrm{d}_{kk}^{t}} = 0, \tag{A 2}$$

and hence

$$\alpha = \pm\frac{6}{7}\left(\frac{2\mathrm{d}_X^{1t}}{\mathrm{d}_{kk}^{t}}\right)^{1/2}. \tag{A 3}$$

For $\bar{A}_0(\tilde{X})$ to remain exponentially small at infinity as we deform the contour off the positive real $\tilde{X}$-axis, we require that

$$\mathrm{Re}\left[\left(\frac{36c}{49}\right)^{1/2}\right] < 0 \tag{A 4}$$

where, for convenience, $c = 2\mathrm{d}_X^{1t}/\mathrm{d}_{kk}^{t}$. As the pressure gradient parameter m changes over the range $-0.09 < m < 0$, c moves in the complex plane as shown in figure 16. We thus take the branch cut to lie in the right-hand half-plane, to avoid discontinuities in $\bar{\omega}_2$.

We now let $\tilde{X} = R\mathrm{e}^{\mathrm{i}\theta}$ and $c = S\mathrm{e}^{\mathrm{i}\phi}$. In the X-plane, we place the branch cut on the aerofoil chord along the negative $\tilde{X}$-axis. Together with the branch cut shown in

https://doi.org/10.1017/S0022112097005314 Published online by Cambridge University Press

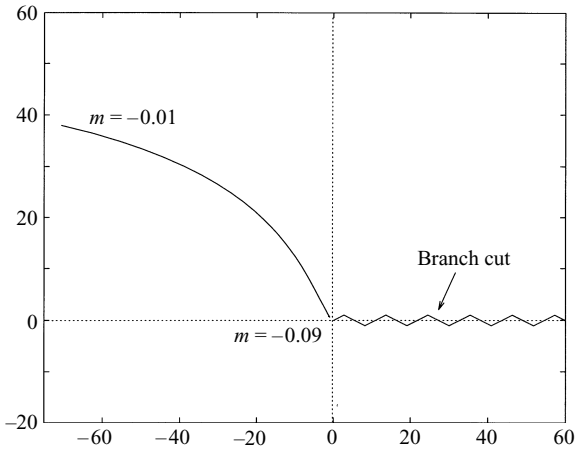

FIGURE 16. Locus of $c = 2\mathrm{d}_X^{1t}/\mathrm{d}_{kk}^{t}$ as m varies, including the branch cut.

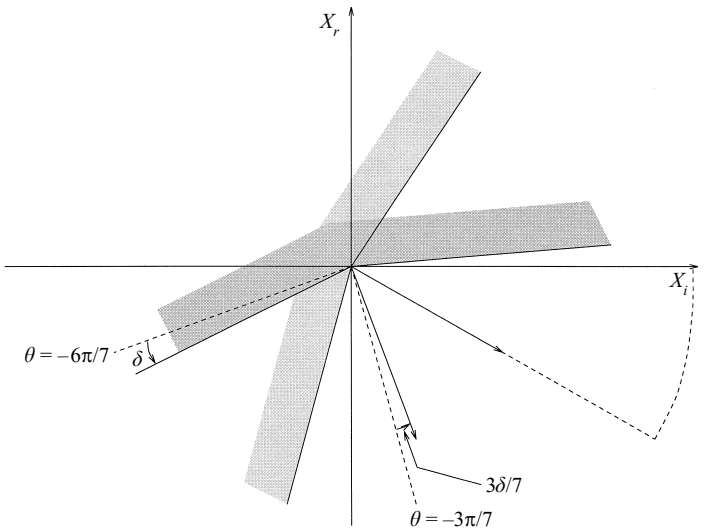

FIGURE 17. X-contour deformation regions. The unshaded region is where the contour may be validly deformed off the positive real axis.

figure 16 this restricts θ and ϕ to the ranges $-\pi < \theta < \pi$ and $0 < \phi < 2\pi$. It should be noted that at the point where c crosses the negative real axis the real part of $c^{1/2}$ changes sign, and hence one must take account of this when taking the plus or the minus sign in (A 3). Since the imaginary part of c is zero at this point, neither solution of (2.41) decays as $\tilde{X}$ tends to infinity. This change of behaviour only takes place though when m is large and negative: for m in the range $-0.089 < m < 0$, c lies in the 2nd quadrant and the problem is well behaved; when c lies in the 2nd quadrant, $\mathrm{Re}[c^{1/2}] > 0$. Hence we must take the minus sign in (A 3), to give the asymptotic behaviour

$$\bar{A}_0 \sim \exp\left[-\tfrac{6}{7}c^{1/2}\tilde{X}^{7/6}\right] \tag{A 5}$$

as $\tilde{X} \to +\infty$ along the real axis. In order to deform the contour off the real X-axis in

https://doi.org/10.1017/S0022112097005314 Published online by Cambridge University Press

such a way that $\bar{A}_0$ remains bounded, we now require that

$$\mathrm{Re}\left[c^{1/2}\tilde{X}^{7/6}\right] > 0, \tag{A 6}$$

and hence that

$$-\frac{\pi}{2} < \frac{\phi}{2} + \frac{7\theta}{6} < \frac{\pi}{2}. \tag{A 7}$$

Substituting $\phi = \pi - \delta$, where $0 < \delta < \pi/2$, we find that θ should lie in the range

$$-(6\pi/7) + (3\delta/7) < \theta < (3\delta/7), \tag{A 8}$$

which, as should be expected, includes the positive real axis $\theta = 0$. Note that the substitution given by (2.42) gives the argument of X as

$$\theta = -(3\pi/7) + (3\delta/7), \tag{A 9}$$

as shown in figure 17. Solving (2.43) for a then gives us the $O(\epsilon^{2/7})$ frequency correction $\bar{\omega}_2$ as

$$\bar{\omega}_2 = \mathrm{d}_X^{1t}\left(\frac{\mathrm{d}_{kk}^{t}}{2\mathrm{d}_X^{1t}}\right)^{1/7} a\ . \tag{A 10}$$

Hence, we have shown that by defining the branch cuts as above we obtain a self-consistent way of performing the transformation, and which results in a unique definition of $\bar{\omega}_2$.

REFERENCES

Acheson, D. J. 1990 *Elementary Fluid Dynamics*. Oxford University Press.

Bers, A. 1975 Linear waves and instabilities. In *Physique des Plasmas* (ed. C. DeWitt & J. Peyraud), pp. 117–215. Gordon & Breach.

Bers, A. 1983 Space-time evolution of plasma instabilities - absolute and convective. In *Handbook of Plasma Physics* (ed. M. N. Rosenbluth & R. Z. Sagdeev), vol. 1, pp. 451–517. North-Holland.

Briggs, R. J. 1964 *Electron-Stream Interaction with Plasmas*. MIT Press.

Daniels, P. G. 1976 A numerical and asymptotic investigation of boundary layer wake evolution. *J. Inst. Maths Applics.* **17**, 367–386.

Goldstein, S. 1930 Concerning some solutions of the boundary layer equations in hydrodynamics. *Proc. Camb. Phil. Soc.* **26**, 1–30.

Huerre, P. & Monkewitz, P. A. 1990 Local and global instabilities in spatially developing flows. *Ann. Rev. Fluid Mech.* **22**, 473–537.

Mattingly, G. E. & Criminale, W. O. 1972 The stability of an incompressible two-dimensional wake. *J. Fluid Mech.* **51**, 233–272.

Monkewitz, P. A., Huerre, P. & Chomaz, J.-M. 1993 Global linear stability analysis of weakly non-parallel shear flows. *J. Fluid Mech.* **251**, 1–20 (referred to herein as MHC 93).

Panton, R. L. 1984 *Incompressible flow*. Wiley.

Papageorgiou, D. T. & Smith, F. T. 1989 Linear instability of the wake behind a flat plate placed parallel to a uniform stream. *J. Fluid Mech.* **208**, 67–89.

Sato, H. & Kuriki, K. 1961 The mechanism of transition in the wake of a thin flat plate placed parallel to a uniform flow. *J. Fluid Mech.* **11**, 321–352.

Schumm, M., Berger, E. & Monkewitz, P. A. 1994 Self-excited oscillations in the wake of two-dimensional bluff bodies and their control. *J. Fluid Mech.* **271**, 17–53.

Smith, F. T. 1974 Boundary layer flow near a discontinuity in wall conditions. *J. Inst. Maths Applics.* **13**, 127–145.

Triantafyllou, G. S. & Karniadakis, G. E. 1990 Computational reducibility of unsteady viscous flows. *Phys. Fluids* A **2**, 653–656.

Woodley, B. M. & Peake, N. 1997 Global linear instability of finite thickness trailing edge wakes. *In preparation.*

https://doi.org/10.1017/S0022112097005314 Published online by Cambridge University Press